Biomaterials Science

Accepted Manuscript

This article can be cited before page numbers have been issued, to do this please use: N. Zandi, E. Mostafavi, M. Shokrgozar, E. Tamjid, T. Webster, N. Annabi and A. Simchi, *Biomater. Sci.*, 2019, DOI: 10.1039/C9BM00668K.

ROYAL SOCIETY OF CHEMISTRY

rsc.li/biomaterials-science

View Article Online
DOI: 10.1039/C9BM00668K

ARTICLE

Biomimetic Proteoglycan Nanoparticles for Growth Factor Immobilization and Delivery

Received 00th January 20xx,
Accepted 00th January 20xx

DOI: 10.1039/x0xx00000x

Nooshin Zandi[a,b], Ebrahim Mostafavi[b], Mohammad Ali Shokrgozar[c], Elnaz Tamjid[d], Thomas. J. Webster[b], Nasim Annabi[*,e,f,g] and Abdolreza Simchi[*,a, h]

The delivery of growth factors is often challenging due to their short half-life, low stability, and rapid disactivation. In native tissues, the sulfated residual of glycosaminoglycan (GAG) polymer chains of proteoglycans immobilizes growth factors through the proteoglycans/proteins' complexation with nanoscale organization. These biological assemblies can influence growth factor-cell surface receptor interactions, cell differentiation, cell-cell signaling, as well as the mechanical properties of the tissues. Here, we introduce a facile procedure to prepare novel biomimetic proteoglycan nanocarriers, based on naturally-derived polymers, for the immobilization and controlled release of growth factors. We developed polyelectrolyte complex nanoparticles (PCNs) as growth factor nanocarriers, which mimic the dimension, chemical composition, and growth factor immobilization of proteoglycans in the native tissue. PCNs were prepared by polymer-polymer pair reaction method and characterized for physicochemical properties. Fourier-transform infrared spectroscopy (FTIR) analysis indicated that complexations occurred through electrostatic interactions. Transmission electron microscopy (TEM) results showed that the nanocarriers had a diameter of 60 ± 11 nm and 91 ± 33 nm for dermatan sulfate sodium salt-poly-l-lysine (DS-PLL) and gum tragacanth-poly-l-lysine (GT-PLL) complexes, respectively. The colloidal nanoparticles were stable due to their negative zeta potential, i.e. -25 ± 4 mV for DS-PLL and -18 ± 3.5 mV for GT-PLL. Cytocompatibility of the PCNs in contact with human bone marrow stromal cells (HS-5) was confirmed by using live/dead assay and metabolic activity measurement. In addition, vascular endothelial growth factor (VEGF) was used to evaluate the ability of the PCNs for the growth factor stabilization. The capability of the PCNs to preserve VEGF activity for up to 21 days was confirmed by analysis the metabolic and mitogenic characteristics of human umbilical vein endothelial cells (HUVECs). Our results demonstrate the potential applications of these nanoparticles for therapeutic delivery for tissue regeneration applications.

Keywords: Biomimetic nanoparticle; proteoglycan; growth factor; glycosaminoglycan

Introduction

During the past decade, considerable efforts have been made to enhance the bioavailability and biocompatibility of therapeutic agents[1]. Among the different delivery carriers, polyelectrolyte complexes have attracted great attention due to their well-tolerated properties and potential as delivery vehicles for drugs, enzymes, proteins, and DNA encapsulation [2].polyelectrolyte complex is appropriate for charged drug molecules loading due to simple fabrication process, high drug loading efficiency and efficacy, acceptable structural stability, and extended circulation in the blood [3].

Polyelectrolyte complex structures are made by complexation of oppositely charged biopolymers in solution at the molecular level, generally via formation of hydrogen bonds, and electrostatic and hydrophobic interactions [4-7]. Electrostatic interactions are important intermolecular forces for complex oppositely charged polymers, which are derived by entropy changes through the release of bound counter ions [8]. Under non-stoichiometric compositions, nanoparticles (NPs) with a net charge of the excess component are formed [9]. Polyelectrolyte complex nanoparticles (PCN) derived from naturally-derived polymers are promising vehicles for active-targeting delivery because natural polymers intrinsically have cell binding sites and exhibit robust

Author information
[a] *Institute for Nanoscience and Nanotechnology, Sharif University of Technology, P.O. Box 11365-11155, Tehran.*
[b] *Department of Chemical Engineering, Northeastern University, Boston, MA, USA† Footnotes relating to the title and/or authors should appear here.*
[c] *National Cell Bank Department, Pasteur Institute of Iran, Tehran 13164, Iran.*
[d] *Department of Nanobiotechnology, Faculty of Biological Sciences Tarbiat Modares University, P.O. Box 14115-175, Tehran, Iran.*
[e] *Department of Chemical and Biomolecular Engineering, University of California-Los Angeles, Los Angeles, California 90095, USA.*
[f] *Center for Minimally Invasive Therapeutics (C-MIT), California NanoSystems Institute (CNSI), University of California – Los Angeles, 570 Westwood Plaza, Los Angeles, CA 90095, USA.*
[g] *Harvard-MIT Division of Health Sciences and Technology, Massachusetts Institute of Technology, Cambridge, MA 02139, USA.*
[h] *Department of Materials Science and Engineering, Sharif University of Technology, P.O. Box 11365-11155, Tehran, Iran.*
[*] *Address correspondence to:*
Nasim Annabi, Tel: (310) 267-5927; E-mail: nannabi@UCLA.edu
Abdolreza Simchi, Tel: +98 (21) 6616; E-mail: simchi@sharif.edu

biocompatibility [10, 11]. For example, negatively charged polysaccharides, such as carboxymethyl cellulose [12], dextran sulfate [13], alginate [3], and chondroitin sulfate [14], have been complexed with positively charged polymers to generate PCN for drug delivery [15].

Glycosaminoglycan (GAG) includes different types of long linear polysaccharide chains containing chondroitin sulfate (CS), keratan sulfate (KS), dermatan sulfate (DS), heparin (HP), hyaluronic acid (HA), and heparin sulfate (HS) [16]. In addition, GAG has various negatively charged carboxyl and sulfate groups that can maintain water in tissue and can be used as therapeutic agents for the treatment of osteoarthritis, cancer, bacterial and viral infections, and blood clotting. These biopolymers can regulate cell signalling, migration, and differentiation through specific interactions with various ligands. Sulfated GAG is often covalently bound to a protein to form proteoglycans (PG), which derives its function from the GAG side chain [17].

In native tissues, growth factor stabilization and delivery to cells are driven by various stimuli through complex microenvironments. Therefore, biomimetic milieu enables growth factor stabilization and delivery, simultaneously. The GAG side chains of different proteoglycans are responsible for growth factor stabilization and protection, as well as signal regulation through linkage with cell surface receptors [18-20]. This motivates the usage of GAG as a carrier for the growth factors. Proteoglycans form a widespread range of sizes, with a core protein ranging from 20 to 400 kDa, and GAG side chains from one or two side chains such as decorin and biglycan to over 100 side chains like aggrecan. These structures display nanoscale organization[21]. Therefore, in addition to chemical functions of proteoglycans, their nanoscale structures play a crucial role in their biophysical function [21-24].

Gum tragacanth (GT) is another biocompatible and biodegradable polysaccharide which has been used for the preparation of delivery vehicles [25]. At near neutral pH, carboxyl groups of GT are dissociated, possessing negative charges to interact with positively charged polymers such as PLL [26]. PLL and its derivatives, as homo-poly-amino acid, are an important class of biodegradable cationic polymers for biomedical and pharmaceutical applications that have extensively been studied and utilized as auxiliary agents in drug delivery systems [27].

Different PCNs have been formed by complexing biopolymers, including combinations of chitosan with different negatively charged polymers such as dextran sulfate [28], hyaluronic [29], alginate [30] or heparin [31]. PCNs could be used to preserve growth factors from degradation by enzyme along with desired release profile. In addition, their nanoscale size allows crossing of the epithelium [32]. Huang *et al.* investigated the mitogenic properties of VEGF using VEGF-PCNs complexation up to five days. They used dextran sulfate as anionic polymer with different polycations including: poly-L-lysine (PLL), chitosan, and poly- (ethyleneimine) to prepare the PCNs [33]. Incorporation of chitosan-heparin NPs with a decellularized vein scaffold was reported in order to promote vascularization in the scaffold through localizing the VEGF. Results revealed that controlled release of VEGF over 30 days could increase cellular proliferation and infiltration, ECM generation, and vascularization [31].

In addition to the excessive attention to other polysaccharides such as heparin [34], dermatan sulfate (DS) functions as a cofactor in a variety of therapeutics, especially in cell-mediated tissue regeneration. This biopolymer plays an important role in binding to and activating extracellular molecules and growth factors for numerous essential biological processes, including cell adhesion, migration, proliferation and differentiation [30]. However, so far, the use of DS in clinical trials is limited in drug delivery platforms for promoting therapeutic functions. Herein, we use VEGF as a model growth factor due to its short circulation half-life, and its binding to PCNs could influence its stability and presentation to growth factor receptors[33, 35]. In addition, it has been reported that modified VEGF with these ECM-binding motifs improved healing in chronic diabetic wounds and bone defects[36].

In the current study, we developed polyelectrolyte NPs that mimic the size and biochemical functions and chemistry of proteoglycans for VEGF protection and immobilization. Biomimetic proteoglycan NPs were prepared through a combination of PLL as the polycationic element and two anionic polysaccharides of GT and Dermatan sulfate sodium salt (DS). The engineered NPs were characterized by size distribution, zeta potential, surface functional groups, and cytocompatibility against human bone marrow stromal cells (HS-5). The ability of the PCNs to preserve VEGF activity was investigated by measuring the metabolic and mitogenic characteristics of human umbilical vein endothelial cells (HUVECs) in the presence of PCNs.

Results and discussion

The nanocarrier was formed by the interaction between the dissociated functional groups: an anionic sulfonate group ($-OSO_3^-$ in dermatan sulfate polymer) and carboxyl group ($-COO^-$ in GT) with a cationic amino group ($-NH_3^+$) from PLL without cross-linking, or the use of surfactant organic solvent. The physical characteristics (hydrodynamic particle size, zeta potential, and poly dispersity index (PDI) of PCNs with different polycation:polyanion mixing ratio in DI water are shown in Table 1. Figure 1 demonstrates a schematic of the chemical building units of the polymers and their interactions to form complex NPs. The process yield was 41 ± 6 % for DS-PLL and 30 ± 5 % for GT-PLL. Zeta potential indicated the negatively charged PCNs (Table 1). The colloidal NPs in DI water were deemed stable due to their negative zeta potential, i.e. of -25 ± 4 mV (DS-PLL) and -18 ± 3.5 mV (GT-PLL). These structures might form a core/shell configuration, where the excess polymer in polyelectrolyte component is located in the shell, giving the particle the defined charge sign and colloid stability. The negatively charged PCNs could easily bind to the positively charged drug and growth factors, which made them suitable candidates for delivery of therapeutics. This method is suitable for encapsulating sensitive materials, which are sensitive to different stress factors such as proteins. The characteristics of the prepared nanocarriers and their potential to immobilize VEGF and preserve the growth factor activity were then studied.

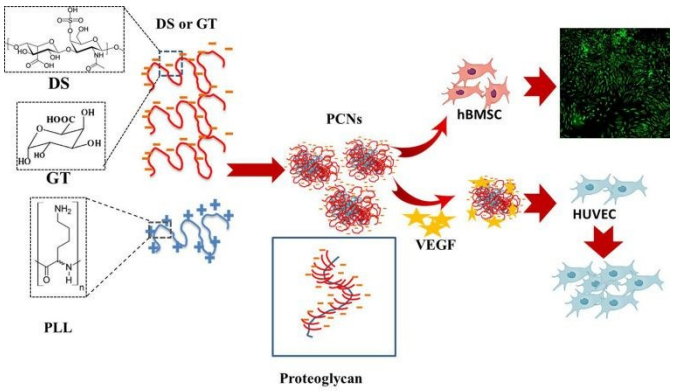

Figure 1. Schematic representation of nanoparticle formation and their interaction with cells. Polyelectrolyte nanoparticles were formed by the complexation of polycationic PLL (blue) with the polyanionic DS or GT (red) in excess. These NPs have similar size and composition of the proteoglycans in the body. PCN were exposed to hBMSCs to evaluate their cytocompatibility. The mitogenic and metabolic activity of immobilized VEGF on the PCN was also evaluated by using HUVECs.

The size and morphology of the PCNs

Representative scanning electron microscopy (SEM) and transmission electron microscopy (TEM) of PCNs and their size distribution histogram are shown in Figure 2a-f. These analyses indicated individual spherical particles with an average diameter of 60 ± 11 nm and 91 ± 33 nm for DS-PLL and GT-PLL NPs, respectively. Also, SEM and TEM images of VEGF-loaded PCNs are shown in Figure 1Sa-d. These analyses indicated individual spherical particles with an average diameter of 55± 8 nm and 103 ± 29 nm for DS-PLL-VEGF and GT-PLL-VEGF NPs, respectively.

Based on the DLS data reported in Table 1, we selected 1:6 and 1:10 as the optimum polycation:polynion mixing ratio for DS-PLL and GT-PLL, respectively due to the optimum values for PDI, hydrodynamic size and zeta potential of NPs. The result showed a hydrodynamic size of 105 ± 0.5 nm for DS-PLL and 220 ± 2 nm for GT-PLL with monomodal size distribution. The larger size of the GT-PLL NPs can be attributed to the higher molecular weight of GT (180 kDa) as compared to DS (84 kDa). It is important to mention that the complex NPs in the solution do not behave like hard spheres, but rather they are gel-like or have a solid core surrounded by a charged corona [37]. TEM can be used to observe the NPs in the dry state; however, dynamic light scattering (DLS) enables to detect the NPs in a solvent. Therefore, DLS method indicates the hydrodynamic diameter of particles, including core with any molecules attached or adsorbed on the surface. Solvent molecules bind to the particles through different non-covalent interactions such as van der Waals interactions, hydrogen bonding or π-π stacking. The size of the particles measured by DLS depends on the type of solvent. Different solvents ensure different solvation characteristics. Water which is PCNs media represents both a hydrogen bond donor and acceptor. The hydrogen bond is a specific type of strong non-covalent interaction that includes dipole-dipole attraction between a partially positive hydrogen atom and a partially negative oxygen, nitrogen, sulfur, or fluorine atom. Therefore, as expected the particle sizes measured by DLS method are slightly bigger than those measured via TEM and SEM images.

On the other hand, the zeta potential of DS-PLL was slightly lower (-25 ± 4 mV) than that of GT-PLL (-18 ± 3.5 mV). This observation indicates that anionic PCNs were formed. Nevertheless, DS has strong anionic sulfate groups while GT is a mild anionic polysaccharide. Therefore, DS-PLL NPs showed a lower zeta potential. The size, PDI, and zeta potential of PCNs after growth factor loading are also reported in Table 2. The magnitude of the zeta potential substantially dropped after incorporation of VEGF in PCNs for both types of PCNs, whereas, the hydrodynamic size of PCNs did not show significant changes after loading of VEGF.

Table 1. Hydrodynamic diameter (Dh, nm), poly dispersity index (PDI), and Zeta potential (ζ, mV) for DS-PLL and GT-PLL PCN prepared at different charge mixing ratios.

$V_{PA}:V_{PC}$	Property	DS-PLL	GT-PLL
1:5	D_h	222±8	402±4
	PDI	0.11±0.02	0.13±0.05
	ζ	-27±4	-20±3
1:6	D_h	105±0.5	376±3
	PDI	0.12±0.05	0.13±0.02
	ζ	-25±4	-19±2.5
1:7	D_h	107±3.5	304±6
	PDI	0.2±0.08	0.32±0.07
	ζ	-21±3	-18.5±3
1:10	D_h	102±9	220±2
	PDI	0.338±0.3	0.22±0.08
	ζ	-19±2	-18±3.5

In addition, DLS analysis of DS-PLL and GT-PLL with 1:6 and 1:10 mixing ratios of polycation:polyanion in cell culture media are reported in Table 2. The average size distribution of the particles suspended in cell culture media was greater than those in DI water. This indicates that PCNs formed larger complexes in media. To that end, the PDI of the particles suspended in media were higher than those suspended in DI water, implying that PCNs in culture media had broader size distributions. Suspension of PCNs in culture media yielded lower surface charge density. The electrostatic binding hypotheses state can explain the interaction between proteins in the culture media and negatively charged PCNs. On the other hand, the lower surface charge density of PCNs in culture media might be derived from adsorption of uncharged or positively charged amino acids (e.g. L-Glutamine in blood serum).

Furthermore, to evaluate the stability of PCNs at the optimized conditions (a concentration of 1 mg/ml in acetate buffer with 0.1 M and pH = 5.5), the hydrodynamic diameter and zeta potential of nanoparticles were measured on days 1, 3 and 14 after incubation at room temperature. As shown in Figure 3, no significant changes in hydrodynamic size of PCNs were observed. In addition, the zeta potential value remained the same after 14 days.

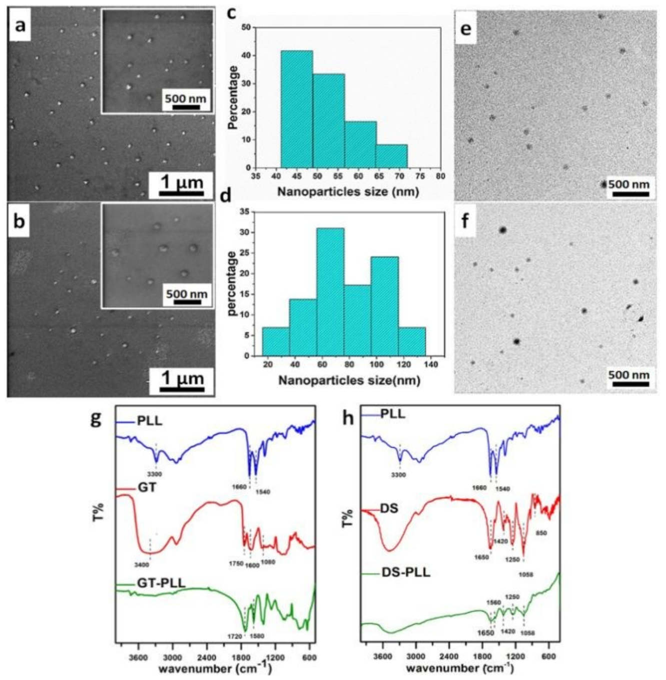

Figure 2. Characterization of PCN. Representative scanning electron microscopy (SEM) images of negatively charged (a) DS-PLL (b) and GT-PLL NPs. Size histograms for (c) DS-PLL and (d) GT-PLL by measuring the mean dimeters of NPs using ImageJ software (National Institute of Health, Bethesda, MD). Representative transmission electron microscopy (TEM) images of (e) DS-PLL and (f) GT-PLL NPs. FTIR spectra of (g) raw materials (DS, PLL, and GT) and the (h) the synthesized NPs.

Table 2. PCN Characterization in DI water and cell culture media.

Particle Media	Composition	Particle size (nm)	PDI	Zeta potential (mV)
DI water	DS-PLL DS-PLL-VEGF	105±0.5 98±7	0.12±0.05 0.28±0.05	-25±4 -11.20±3
	GT-PLL GT-PLL-VEGF	220±2 212±9	0.22±0.08 0.36±0.03	-18±3.5 -5±2
Cell culture media	DS-PLL	118.6±4.1	0.411±0.04	-11.43±3
	GT-PLL	290±3.5	0.324±0.06	-5.17±3.8

Fourier-transform infrared spectroscopy

FTIR spectra of pristine GT, PLL, and DS polymers and the complex FTIR spectra of NPs (GT-PLL and DS-PLL) are shown in Figures 2g-h. Two features are prominent in the spectrum of PLL including absorbance in the range 3300 cm^{-1} and the bands near 1500-1600 cm^{-1}. The band at 1620–1700 cm^{-1} was attributed to amide I (mainly CO stretching mode) and the band at 1540 cm^{-1} (amide II) was related to the in-plane deformational mode of the NH group [38]. Both bands were related to the vibrational modes of the peptide group. Bands at 1650 and 1429 cm^{-1} in the FTIR spectrum of DS were related to axial symmetrical and asymmetrical deformations of carboxylate anions, respectively [39]. The bands at 1250 and 850 cm^{-1} were attributed to the axial asymmetry of S=O groups and to the axial deformation of C–O–S [40]. Major absorbance bands in GT appeared at 3415 cm^{-1} (stretching vibrations of O-H groups), 2945 cm^{-1} (stretching vibrations of methylene groups), 1750 cm^{-1} (various carbonyl species), 1620 cm^{-1} (carbonyl stretching vibrations in carboxylic acids), 1417 cm^{-1} (symmetrical stretch of carboxylate group), 1244 and 115 cm^{-1} (C-O stretching vibrations of polyols), and 1080 and 1024 cm^{-1} (C-O stretching vibrations of ether and alcohol groups) [37]. After complexation, peak shifts, the appearance of new peaks and/or disappearance of some characteristic peaks, were observed.

In DS-PLL, shifting of the band at 1660 cm^{-1} to 1560 cm^{-1} was observed due to vibrations of the residual $N–H^+$ bonds in PLL. Based on a previous study [41], electrostatic interactions between PLL and DS can be verified over spectra analysis at 1520 to 1560 cm^{-1}. These bands in the FTIR spectra of PCN showed reduced intensity. The complexation of COO^- in the DS chains with cationic moieties in PLL polymer chains can be an explanation of this effect. Electrostatic interactions between NH_3^+ of PLL with $–OSO_3^-$ groups of DS contributed to the formation of an anionic-cationic polymer complex. Additional evidence could be the disappearance of the band at 850 cm^{-1} for DS after complexation. Instead, the intensity of a 1250 cm^{-1} band was enhanced as compared to DS. Similar changes were noticed in the FTIR spectrum of GT-PLL. The complexed material showed a narrower band around 3300 cm^{-1}, due to new hydrogen bonds forming between –OH and $–NH_2$ functional groups of PLL and –C=O and –OH functional groups of GT [42]. On the other hand, the bands assigned to motions of $–NH_2$ at 3300 cm^{-1} became invisible after complexation. This disappearance could be related to the lower content of PLL and GT excess in the complex NPs. Intense peaks at around 1580 cm^{-1} and 1720 cm^{-1} were also present. The peak at 1720 cm^{-1} probably corresponded to asymmetric stretching of $–COO^-$ groups that might indicate polyelectrolyte complex development. From FTIR spectroscopy, it can be concluded that ionic bonds between PLL amine groups and the carboxyl group of GT were formed, which is in agreement with a previous study [43].

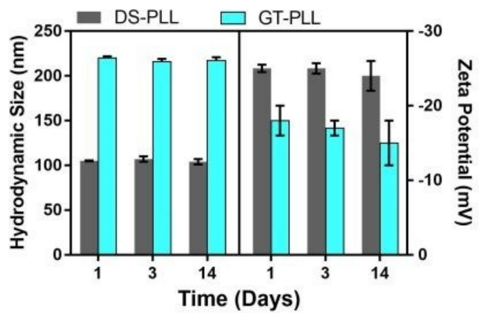

Figure 3. Hydrodynamic diameter (nm) and zeta potential (mV) for DS-PLL and GT-PLL PCNs after 1, 3, and 14 days of incubation in acetate buffer (pH = 5.5) at room temperature (25˚C).

Cytocompatibility assays

To determine the *in vitro* cytocompatibilty of PCNs, Live/Dead assays and metabolic activity measurement were performed after exposing Human bone marrow stromal cell line (HS-5) to the engineered PCNs. Three doses of PCNs (200, 400, and 800 μg mL^{-1}) were compared to the untreated cells as a negative control (cells in the culture medium without the NPs). Representative live/dead stained images of cells treated with PCNs as compared with the controls are demonstrated in Figure 4a. The Live/Dead assay stains the dead cells in red and the live cells in green. For both type of PCNs, the viability significantly decreased (to less that 50% cell viability), the concentration of NPs increased to higher 400 μg mL^{-1}. This drop in cell viability at higher concentration indicates their cytotoxicity at high concentration (Figure 4b).

A PrestoBlue® assay was carried out to evaluate cellular metabolic activity at three dose levels of 200, 400 and 800 μg mL^{-1}, at days 1, 3 and 5 post culture. As shown in Figure 4c, no statistical difference between the NPs at 200 μg mL^{-1} and control was observed. Additionally, the results revealed that at higher concentrations of NPs (e.g. 400 and 800 μg mL^{-1}), the metabolic activity of the cells decreased consistently during 5 days of culture. At NPs concentration higher than of 400 μg mL^{-1}, the NPs could prevent attachment of the cell to the surface of the well plate. In addition, these NPs may also have cytotoxic effects toward cells at higher concentrations.

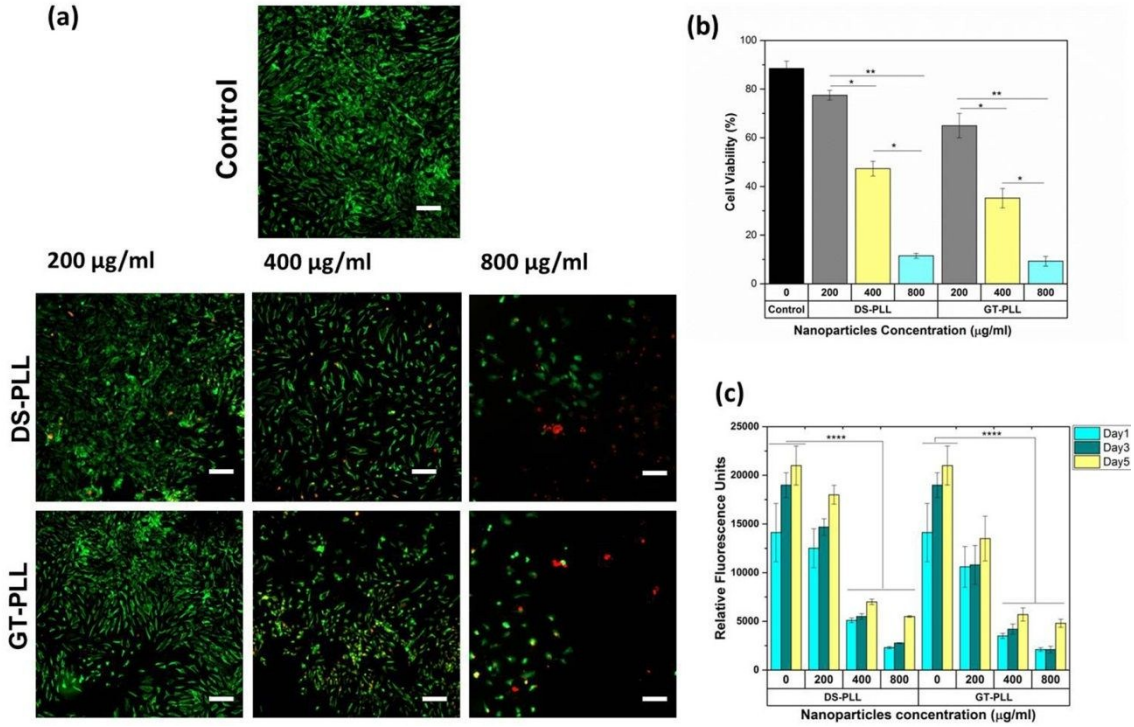

Figure 4. ***In vitro*** **cytocompatibility of the polyelectrolyte NPs against HS-5 cell.** (a) Representative Live/Dead stained images indicating the effect of PCNs (DS-PLL and GT-PLL) dose on the cell viability at day 3 post seeding. The concentration increases from 200 to 800 μg mL^{-1} from left to right. Cytotoxicity was observed for the cells treated with NPs at concentrations >400 μg mL^{-1}. (b) Quantification of cell viability after 24 h of incubation. (c) Quantification of metabolic activity of hBMSCs was based on relative fluorescence units (RFU) assayed after different incubation times (1, 3 and 5 days post seeding). Scale bars: 100μm. Results are presented as the mean ± STD with at least three replicates per group/ The minimal level of significance chosen was p<0.001. The Significance levels are shown as $p < 0.05$ (*), $p < 0.01$ (**), $p < 0.001$ (***) and $p < 0.0001$(****) for n=3.

Cell Response to VEGF and preconditioned VEGF-Loaded PCNs

The ability of PCNs to preserve VEGF activity was evaluated by exposing the preconditioned VEGF-loaded PCNs, and uncomplexed VEGF for 7 and 14 days to HUVECs at 37 °C in culture media. We used 10 ng mL^{-1} VEGF and 100 μg mL^{-1} PCNs as the final concentrations. The VEGF loading efficiency was 93.1 ± 5 % and 80.2 ± 3 % for DS-PLL, and GT-PLL, respectively. Since there was no step to remove free VEGF, each experiment (mitogenic and methabolic activity experiments) uses an equal amount of VEGF.

Regarding the negative control (no VEGF), HUVECs did not proliferate in this low-serum condition after 48 h of cell culture. Representative DAPI-stained images in Figure 5a show fluorescence images of cell nuclei culturing in low-serum media for both VEGF bound to PCNs (DS-PLL and GT-PLL), and VEGF in solution after 7 and 14 days. The number of cells was normalized and compared for both form of VEGF bound to PCNs and free VEGF in Figure 5b. As the results show, untreated cells did not proliferate the in the low-serum media. Cell proliferation was observed for free VEGF but was significantly lower than that of the treated cells with PCN-bound VEGF. The normalized cell numbers for the free VEGF was statistically lower than the VEGF bound to PCNs (for both DS-PLL and GT-PLL) in both preconditioning times. However, these values were not statistically significant compared to the negative control.

In addition, the normalized cell numbers were all more than 1 for both of the treatments with VEGF (bound and free VEGF), indicating cell numbers were enhanced as compared to the cells cultured without the growth factor. The mitogenic activity of VEGF bound to DS-PLL was also more than that of VEGF bound to GT-PLL at each time point. It can be concluded that treatment with VEGF bound to PCNs (for both DS-PLL and GT-PLL) represent mitogenic activity over the 14 days preconditioning in the high level, while the result showed that free VEGF lost some of their mitogenic activity by increasing the preconditioning time.

The MTT assay was used to investigate the cellular responses to the preconditioned VEGF (7, 14, or 21 days) during mitosis experiments for 48 h. Figure 5c demonstrates the results of the metabolic activity for both types of VEGF-containing treatments. The VEGF-bound to each type of PCNs demonstrated no statistical differences over all preconditioning time. This result indicates that based on metabolic activity of treatments, VEGF activity did not change during preconditioning time. However, free VEGF treatment showed a significant reduction in metabolic activity after 21 days in comparison to 7 days of preconditioning. At day 7 of preconditioning, there was no statistical difference between free and treated VEGF groups. However, by increasing the preconditioning time, loss of metabolic activity of HUVECs was observed. VEGF-bound DS-PLL resulted a higher metabolic activity in comparison to the free VEGF even after 14 days of incubation, but there was no significant difference between VEGF-bound GT-PLL and free VEGF at this time point. Finally, after 21 days of preconditioning time, the metabolic activity of both PCNs treatments was greater than the VEGF alone.

Since free VEGF in solution exhibited a significant lower mitogenic and metabolic activity compared to VEGF bound to both types of PCNs, the PCNs could be mainly responsible for the high level activity of the growth factor. For the DS-PLL PCNs, considerable VEGF molecules could be linked to the PCNs over the preconditioning time which corresponds to higher mitogenic activity of this treatment. In addition, both PCNs treatments induce more metabolic activity at all preconditioning times compared to the negative control, indicating that VEGF remained active during the 21 days (Figure 5c). Both GT and DS biopolymers are highly negatively charged polysaccharides that can bind VEGF electrostatically. However, the glycosaminoglycan used in this work consisted of primarily 6-Osulfated hexosamine and iduronic residue, which are important for binding to VEGF [44, 45], and lack the particular VEGF-binding sulfation, making GT less effective at stabilizing VEGF.

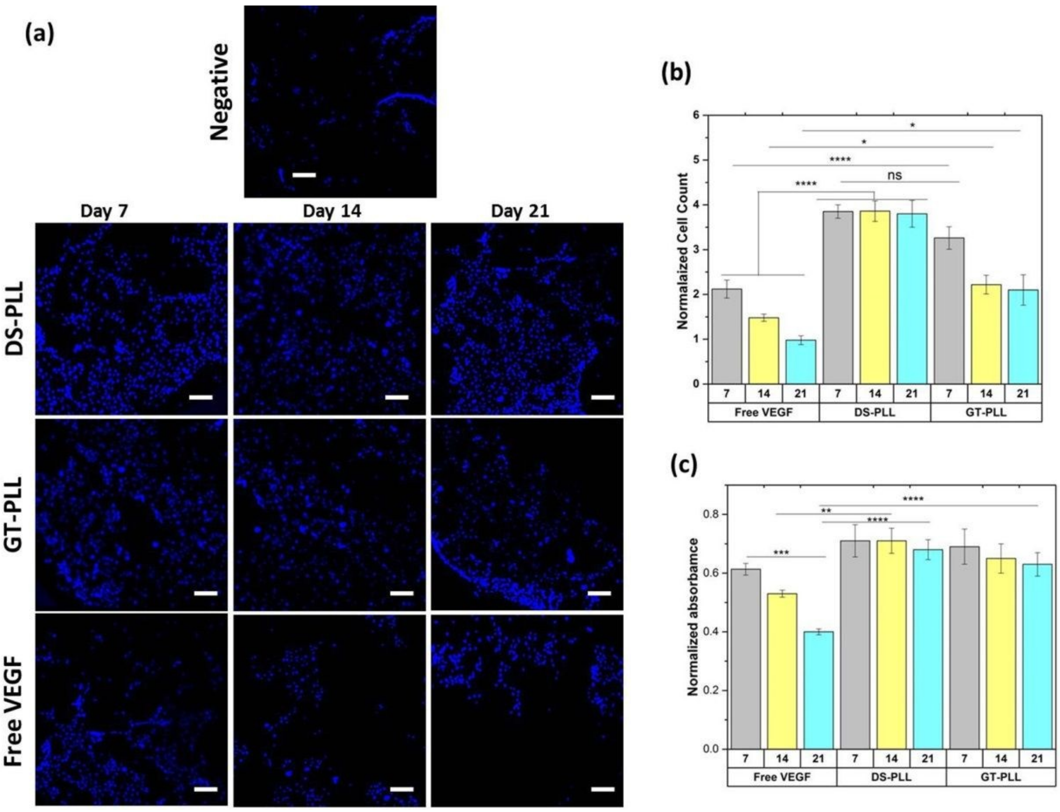

Figure 5. Cell Response to VEGF, and Preconditioned VEGF-Loaded PCNs through mitogenic and metabolic measurements. (a) Representative fluorescence images of HUVEC nuclei stained using DAPI after two days of culture with no treatment (negative control), VEGF-loaded PCNs (DS-PLL and GT-PLL), and free VEGF. Preconditioning time does not show a significant influence on mitogenic activity, but, treatments exhibit significant effect. (b) Quantification of VEGF mitogenic activity after 2 days HUVECs culture for VEGF-loaded PCNs, and free VEGF. The numbers represent cell count normalized to cell counts from the negative control. (c) The Quantification of Metabolic activity after 2 days of culture with VEGF-loaded PCNs, and free VEGF in solution (at different preconditioning time in media up to 21 days). Metabolic activity result was normalized to the metabolic activity of untreated HUVEC cells. Scale bars: 100μm. results were presented as the mean ± SEM with at least three replicates per group The minimal level of significance chosen was p<0.001. The Significance levels are shown as p < 0.01 (**),p < 0.001 (***), and p < 0.0001(****) for n=3.

View Article Online
DOI: 10.1039/C9BM00668K

Experimental

Materials

DS (from porcine intestinal mucosa, ≥90%, lyophilized powder 60 kDa; PDI = 1.94) and PLL (0.1 % (w/v) in H2O) were purchased from Sigma-Aldrich (St. Louis, MO, USA). Sodium acetate, sodium chloride, potassium chloride, sodium phosphate dibasic, and potassium phosphate monobasic were purchased from Merck (Germany). GT used in this study was a high-quality ribbon type, collected from the stems of Fluccosus species of Astragalus bushes, growing in the central areas of Iran. A LIVE/DEAD viability/cytotoxicity kit for mammalian cells was purchased from Invitrogen (Eugene, OR). PrestoBlue reagent and Dulbecco's Phosphate Buffered Saline (DPBS) were purchased from Thermo Fisher Scientific. VEGF was purchased from R&D Systems, MTT (3-[4,5-dimethylthiazol-2-yl]-2,5-diphenyltetrazolium bromide) ,4′,6-Diamidino-2-phenylindole (DAPI), bovine serum albumin (BSA), paraformaldehyde were purchased from Sigma-Aldrich (St. Louis, MO, USA).

Preparation of PCNs

PCNs were prepared through the drop by drop mixing of a polycation solution with a polyanion solution and stirring vigorously with an excess amount of the polyanion. Two different combinations of polycation-polyanion were used to form PCNs including: dermatan sulfate with poly-l l-ysine (DS-PLL), and gum tragacanth with poly-l-lysine (GT-PLL). For DS-PLL NPs, DS (1.8 mg mL^{-1}) and PLL (1 mg mL^{-1}) each solution was prepared by dissolving the biopolymers in acetate buffer (0.1 M and pH = 5.5) under magnetic stirring. The solutions were then filtered by using syringe filters (0.22 µm, Fisher Scientific, PA) to remove particles, precipitates, and undissolved powders. The PLL solution was then added drop by drop to DS in excess at different polycation:polyanion volume ratios (1:5, 1:6, 1:7 and 1:10) under vigorous stirring.

A similar procedure was used for GT-PLL with some modifications: PLL (1 mg mL^{-1}) was mixed with GT (1.8 mg mL^{-1}) at different polycation:polyanion volume ratios (1:5, 1:6, 1:7 and 1:10). The mixtures were left for 24 h to settle and to separate the aggregated part. The supernatant solutions were decanted, centrifuged at 12,000 rpm for 15 min and finally, the precipitates were freeze-dried (vacuum: 9Pa, -50ºC; LaBCONCO, USA). Production yield was determined based on the mass of dried PCNs relative to the dry mass of the starting polymers.

Material characterization

Size and morphology of PCN NPs were examined by scanning electron microscopy (SEM, TEscan, MIRA3, Czech Republic) and transmission electron microscopy (TEM, Zeiss - EM10C). Theried NPs were dispersed in DI water to attain dilute suspensions. For SEM imaging, the suspensions were located onto an aluminum foil, and left to dry at room temperature and gold-coated by an Edwards Sputter Coater (DST1-2, Nanostructured Coatings Co., Iran). SEM images were taken at 2 kV. The mean diameter of the NPs were calculated by measuring the diameter of at least 50 random NPs for each sample from their SEM images using the Image J software (National Institute of Health, Bethesda, MD).

For TEM imaging, a drop of the diluted suspension was placed on a copper-coated grid (Formvar/Carbon 200 mesh, Copper) and TEM analysis was performed at 80 kV. The hydrodynamic size distribution of the NPs was determined using dynamic light scattering (Zetasizer Ver. 6.00, MALVERN, UK) in DI water and cell culture media (α-MEM). The surface charge of the PCNs in DI water at 25°C was measured using a ZetaPALS instrument (Zetasizer Ver. 6.00, MALVERN, UK) in both DI water and cell culture media (α-MEM). Fourier transformed infrared (FTIR) spectra of the NPs were recorded by a Perkin-Elmer instrument (RX, USA) between 450 and 4000 cm^{-1} with a resolution of 1 cm^{-1}.

Cytocompatibility

HS-5 cells from human bone marrow/stroma (obtained from ATCC, Manassas, USA) were cultured at 37 °C and 5 % CO_2 and humidified atmosphere in Minimum Essential Medium α (α-MEM, Gibco, Thermo Fisher Scientific). The media was supplemented with FBS (10 %v/v) and penicillin/streptomycin (1 %v/v). At 70% confluency, the cells were used for evaluation of cell viability and metabolic activity. The biocompatibility of different concentrations of PCNs (200, 400 and 800 µg mL^{-1}) towards HS-5 cells was evaluated through cell viability and metabolic activity assessments.

To evaluate the cell viability in contact with PCNs, a commercial Live/dead assay kit was used[46, 47]. To do this, cells were first seeded in a 24-well plate the density of 20,000 cells/cm^2 and then 1 mL of α-MEM containing 10% FBS was added to each well. The cells were allowed to attach for 4 h. PCNs, DS-PLL, and GT-PLL were then diluted with α-MEM to 3 different concentrations (200, 400, and 800 µg mL^{-1}). After cellular attachment, the resulting solutions were added to the cells. The untreated cell-seeded wells were used as the control. Cells were then incubated at 37 °C and 5% CO_2 for 24 h. The media was aspirated, followed by washing three times with DPBS before Live/Dead staining.

To perform live/dead assay, cells were stained with ethidium homodimer- 1 (EthD-1, 2µl/ml in DPBS) for dead cells and Calcein AM (0.5µl/ml in DPBS) for live cells. 400 µL of dye solution was added to each well and the plates were incubated in the culture incubator for 15 min at 37 °C. For each well, three images were taken by an inverted fluorescence microscope (Zeiss Axio Observer Z1), live and dead cells were counted by the ImageJ software, and the viability was reported by calculating of the number of live cells divided by the total cell number containing live and dead cells.

The measurement of metabolic activity of cells was performed on days 1, 3, and 5 using a PrestoBlue® assay according to the manufacturer's protocol. Briefly, cell treated with PCNs were incubated with a solution containing 10% PrestoBlue® reagent and 90% cell culture medium for 45 min at 37 °C. The final fluorescence was recorded at 535-560 nm excitation and 590-615 nm emission. Relative fluorescence values were calculated and reported for each time point.

Formation of VEGF loaded PCNs

VEGF in DPBS was added to PCN solutions (1 mg mL^{-1}) to make 100 ng mL^{-1} final concentration of growth factor under stirring for 30 min. The growth factor loaded PCNs were then centrifuged (9000 rcf for 10 min). The supernatants were diluted to obtain VEGF concentration in the range of the ELISA. To evaluate the VEGF loading efficiency with the PCNs, an ELISA VEGF kit (R&D System, PeproTech, USA) was used. The growth factor bound to PCNs was

measured by subtracting the VEGF concentration in the supernatants from the initial loaded VEGF in the solution.

Culture of HUVECs

HUVECs (CC-2519, Lonza Group, Basel, Switzerland) were cultured at 37 °C, 5 % CO_2, and humidified atmosphere in EGM-2. The basal medium (not supplemented with VEGF, EGF, bFGF, and IGF) was used to evaluate cell metabolic and mitogenic behavior.

Pre-conditioning VEGF and VEGF-loaded PCNs

To investigate the capability of PCNs to immobilize VEGF, VEGF-loaded PCNs and unbound (free) VEGF were first pre-conditioned through incubation in cell culture media containing 10% FBS at different time points (7, 14, or 21 days and 37 ˚C) to destabilize the VEGF. Finally, the activity of VEGF was evaluated through investigating the mitosis and metabolic ability of HUVECs in low serum media to prevent the interaction between the different compositions in the cell culture media with the growth factors that should be tested. The same procedure (described in VEGF loaded PCNs) was used to load VEGF to each PCN type (DS-PLL and GT-PLL) without centrifugation.

Cell response to unbound VEGF, and VEGF-Loaded PCNs

To evaluate the ability of PCNs to stabilize growth factor, HUVEC cells were cultured in the presence of free and bound VEGF in low-serum cell culture media. HUVECs mitogenic property was assayed after 48 h of culture using the DAPI staining, imaging and counting the nuclei. Finally, metabolic activity of treated cells was assessed by the MTT assay after 48 h of culture.

Mitogenic Activity Assay. The HUVEC proliferation assay was performed to indicate the activity of preconditioned VEGF after 7 and 14 days in cell culture media at 37 °C. The cell density was at 3000 cells cm^{-2} and there samples were tested for each treatment (preconditioned VEGF-loaded PCNs, and free VEGF). Firstly, the cells incubated for 2 h to allow them to attach to the surface of the plate by adding 0.5 mL of untreated media containing 10 % FBS in a 48-well plate. The seeding media was then aspirated and replaced with 0.5 mL of low-serum media containing preconditioned VEGF-loaded PCNs and free VEGF. PCNs treatments were diluted using low serum media to 100 µg mL^{-1} (PCN) containing 10 ng mL^{-1} VEGF final concentration. Free VEGF treatment was also diluted to 10 ng mL^{-1}. The cells nuclei were stained using 4′,6- Diamidino-2-phenylindole (DAPI). Briefly, the cells were fixed in 4% (v/v) paraformaldehyde (Sigma) for 20 min and then permeabilized with 0.1% (w/v) Triton X-100 solution in DPBS for 45 min. Next, 1% (w/v) bovine serum albumin (BSA) solution in DPBS was used to block the samples for 20 min. samples were stained with 1 µL/mL DAPI in DPBS for 5 min and washed three times with DPBS. The stained cells samples were kept at 4 °C in the dark until taking the images. Three nonoverlapping images were taken from each sample. The ImageJ software (National Institutes of Health, U.S.A.) was used to process the images. The cell number per area was calculated using the counting of the cell nuclei by the particle analyzer algorithm in the ImageJ software. Finally, The VEGF activity was recorded as the mean cells numbers per area of each samples, and normalized through the average cells per area in the untreated samples as a control (without VEGF).

Metabolic Activity Measurement. To investigate the effect of VEGF on the cells, the metabolic activities of cells were evaluated by MTT assay at days 7, 14, and 21 after preconditioning periods. All treatments were conducted in triplicates with the cell seeding density of 10^4 cells cm^{-2}. The cells were incubated for 2 h to attach to the surface of well plates with 0.5 mL of non-treated media supplemented with 10% FBS. The media was taken and replaced with 0.5 mL of low-serum media containing the treatment (preconditioned VEGF-binded to each type of PCNs, and free VEGF). All treatments were added to media to obtain the same final concentrations in mitosis assay as explained before. The MTT assay was performed according to the manufacturer's instructions after 48 h of culture. Finally, the VEGF activity was reported as the average of all readings for each sample, and then normalized based on the negative control (no VEGF).

Conclusions

The biomimetic proteoglycan PCNs were developed using a polymer-polymer pair interaction based on cationic (PLL) and anionic (DS and GT) polymers with no use of cross-linking, surfactant and organic solvents or further chemical functionalization to bind the growth factor. The negatively charged PCN can easily bind to the positively charged drug and growth factors, which makes them suitable candidates for the delivery of therapeutics. It was shown that at concentrations of 200 µg mL^{-1} and above, the NPs could prevent attachment of the cells to well plates, and at higher concentrations, they may show cytotoxic effects toward HS-5 cells. The result also determined the time and dose-dependence HS-5 cells metabolic activity.

The result confirmed that the mitogenic activity of VEGF is maintained bound well to DS-PLL PCNs. Free VEGF in solution doesn't show significant mitogenic properties during all incubation periods (normalized cell counts are not significantly greater than 1 for free VEGF). Additionally, during the equal preconditioning time periods, delivery of VEGF using both types of PCNs show higher metabolic activity compared to free VEGF. This could enhance the prospects for delivery of therapeutic using nanoparticle immobilized growth factors or cytokines for tissue regeneration application.

Conflicts of interest

There are no conflicts to declare.

Acknowledgements

AS wish to thank funding support from Sharif University of Technology (Grant No. QA970816) and Iran National Science Foundation (INSF No. 95-S-48740). NA acknowledge the support from National Institutes of Health (NIH) (R01EB023052; R01HL140618).

References

1. M. Uehara, X. Li, A. Sheikhi, N. Zandi, B. Walker, B. Saleh, N. Banouni, L. Jiang, F. Ordikhani and L. Dai, *Scientific reports*, 2019, **9**, 6535.
2. V. Bourganis, T. Karamanidou, O. Kammona and C. Kiparissides, *Eur J Pharm Biopharm*, 2017, **111**, 44-60.
3. R. K. Das, N. Kasoju and U. Bora, *Nanomedicine: Nanotechnology, Biology and Medicine*, 2010, **6**, 153-160.
4. Y. A. Shchipunov and I. V. Postnova, *Composite interfaces*, 2009, **16**, 251-279.

5. Q. Hu, T. Wang, M. Zhou, J. Xue and Y. Luo, *International journal of biological macromolecules*, 2016, **92**, 812-819.
6. R. Poojari, S. Kini, R. Srivastava and D. Panda, *Colloids and Surfaces B: Biointerfaces*, 2016, **143**, 131-138.
7. E. Mostafavi, P. Soltantabar and T. J. Webster, in *Nanotechnology and picotechnology: A new arena for translational medicine*, Academic Press, 2019, pp. 191-212.
8. F.-G. Wu, Y.-W. Jiang, Z. Chen and Z.-W. Yu, *Langmuir*, 2016, **32**, 3655-3664.
9. J.-F. Gohy, S. K. Varshney and R. Jérôme, *Macromolecules*, 2001, **34**, 2745-2747.
10. M. M. Stevens and J. H. George, *Science*, 2005, **310**, 1135-1138.
11. Y. Parajó, I. d'Angelo, A. Welle, M. Garcia-Fuentes and M. J. Alonso, *Drug delivery*, 2010, **17**, 596-604.
12. S. Kaihara, Y. Suzuki and K. Fujimoto, *Colloids and Surfaces B: Biointerfaces*, 2011, **85**, 343-348.
13. A. Anitha, V. Deepagan, V. D. Rani, D. Menon, S. Nair and R. Jayakumar, *Carbohydrate Polymers*, 2011, **84**, 1158-1164.
14. M. A. Shahbazi, M. Hamidi and S. Mohammadi-Samani, *Journal of Pharmacy and Pharmacology*, 2013, **65**, 1118-1133.
15. C. Tan, J. Xie, X. Zhang, J. Cai and S. Xia, *Food Hydrocolloids*, 2016, **57**, 236-245.
16. U. Lindahl and L. Kjellén, *Journal of internal medicine*, 2013, **273**, 555-571.
17. D. M. Copolovici, K. Langel, E. Eriste and U. Langel, *ACS nano*, 2014, **8**, 1972-1994.
18. G. Frescaline, T. Bouderlique, M. B. Huynh, D. Papy-Garcia, J. Courty and P. Albanese, *Stem cell research*, 2012, **8**, 180-192.
19. R. Duschinsky and E. Pleven, *J. Am. Chem. Soc*, 1957, **79**, 4459-4463.
20. D. Berry, C.-P. Kwan, Z. Shriver, G. Venkataraman and R. Sasisekharan, *The FASEB Journal*, 2001, **15**, 1422-1424.
21. S. Boddohi and M. J. Kipper, *Advanced materials*, 2010, **22**, 2998-3016.
22. A. Papagiannopoulos, T. Waigh, T. Hardingham and M. Heinrich, *Biomacromolecules*, 2006, **7**, 2162-2172.
23. C. B. Knudson and W. Knudson, 2001.
24. J. J. Zoeller, J. M. Whitelock and R. V. Iozzo, *Matrix Biology*, 2009, **28**, 284-291.
25. A. Nasirpour, M. Amir, Z. Hajihashemi and M. Fazilati, *International Food Research Journal*, 2013, **20**.
26. M. A. Mohammadifar, S. M. Musavi, A. Kiumarsi and P. A. Williams, *International Journal of Biological Macromolecules*, 2006, **38**, 31-39.
27. J. Kuchlyan, D. Banik, A. Roy, N. Kundu and N. Sarkar, *The Journal of Physical Chemistry B*, 2015, **119**, 8285-8292.
28. B. Sarmento, A. Ribeiro, F. Veiga and D. Ferreira, *Colloids and Surfaces B: Biointerfaces*, 2006, **53**, 193-202.
29. A. Mohandas, B. Anisha, K. Chennazhi and R. Jayakumar, *Colloids and Surfaces B: Biointerfaces*, 2015, **127**, 105-113.
30. Y. Wen, L. Grøndahl, M. R. Gallego, L. Jorgensen, E. H. Møller and H. M. Nielsen, *Biomacromolecules*, 2012, **13**, 905-917.
31. Q. Tan, H. Tang, J. Hu, Y. Hu, X. Zhou, Y. Tao and Z. Wu, *International journal of nanomedicine*, 2011, **6**, 929.
32. S. Rodrigues, M. Dionísio, C. R. López and A. Grenha, *Journal of functional biomaterials*, 2012, **3**, 615-641.
33. M. Huang, S. N. Vitharana, L. J. Peek, T. Coop and C. Berkland, *Biomacromolecules*, 2007, **8**, 1607-1614.
34. N. Perrimon and M. Bernfield, *Nature*, 2000, **404**, 725.
35. S. D. Kingma, T. Wagemans, L. IJlst, A. L. Bronckers, T. H. van Kuppevelt, V. Everts, F. A. Wijburg and N. van Vlies, *Bone*, 2016, **88**, 92-100.
36. J. J. Green and J. H. Elisseeff, *Nature*, 2016, **540**, 386.
37. S. Safi, M. Morshed, S. Hosseini Ravandi and M. Ghiaci, *Journal of applied polymer science*, 2007, **104**, 3245-3255.
38. M. Rozenberg and G. Shoham, *Biophysical chemistry*, 2007, **125**, 166-171.
39. A. F. Martins, J. F. Piai, I. T. Schuquel, A. F. Rubira and E. C. Muniz, *Colloid and Polymer Science*, 2011, **289**, 1133-1144.
40. D.-W. Tang, S.-H. Yu, Y.-C. Ho, F.-L. Mi, P.-L. Kuo and H.-W. Sung, *Biomaterials*, 2010, **31**, 9320-9332.
41. Y.-L. Chen, H.-P. Lee, H.-Y. Chan, L.-Y. Sung, H.-C. Chen and Y.-C. Hu, *Biomaterials*, 2007, **28**, 2294-2305.
42. M. G. Sankalia, R. C. Mashru, J. M. Sankalia and V. B. Sutariya, *European journal of pharmaceutics and biopharmaceutics*, 2007, **65**, 215-232.
43. E. Kokufuta, K. Ogawa, R. Doi, R. Kikuchi and R. S. Farinato, *The Journal of Physical Chemistry B*, 2007, **111**, 8634-8640.
44. M. Lyon, J. A. Deakin, K. Mizuno, T. Nakamura and J. T. Gallagher, *Journal of Biological Chemistry*, 1994, **269**, 11216-11223.
45. E. Wijelath, M. Namekata, J. Murray, M. Furuyashiki, S. Zhang, D. Coan, M. Wakao, R. B. Harris, Y. Suda and L. Wang, *Journal of cellular biochemistry*, 2010, **111**, 461-468.
46. E. Shirzaei Sani, R. Portillo-Lara, A. Spencer, W. Yu, B. M. Geilich, I. Noshadi, T. J. Webster and N. Annabi, *ACS Biomaterials Science & Engineering*, 2018, **4**, 2528-2540.
47. E. S. Sani, A. Kheirkhah, D. Rana, Z. Sun, W. Foulsham, A. Sheikhi, A. Khademhosseini, R. Dana and N. Annabi, *Science Advances*, 2019, **5**, eaav1281.